Integrating Grid impedance estimation method into Advanced Angle Estimation Kalman Filter in GFL inverter

Phuoc Sang Nguyen, *Student Member, IEEE,* Ghavameddin Nourbakhsh, *Member, IEEE,* and Gerard Ledwich, *Life Fellow, IEEE*

***Abstract*—The growing integration of power electronic converter-interfaced distributed energy resources into modern power systems presents significant challenges for system monitoring, protection, and control. Grid impedance plays a critical role in the operation and stability assessment of grid-connected inverter systems. This study presents a real-time grid impedance estimation method based on the Discrete Fourier Transform. The proposed method is integrated with the Advanced Angle Estimation Kalman Filter using a Linear Quadratic Regulator current controller (AAEKF-LQR), assisting the use of impedance information for accurate instantaneous phase angle estimation. Simulation results confirm that the proposed impedance estimation method interacts effectively with the AAEKF-LQR controller, maintaining stable system performance under weak grid conditions. The approach also demonstrates the ability to deliver fast and accurate impedance estimation during operational variations in grid conditions, thereby supporting stable inverter operation.**

***Index Terms*—Grid-following inverter, Kalman Filter, grid impedance estimation, phase angle estimation, high grid impedance.**

I. Introduction

In recent years, the increasing penetration of converter-based distributed energy resources (DERs), such as solar photovoltaics, wind turbines and battery storage, has transformed the landscape of power grid. This shift toward more sustainable energy systems has led to a significant number of converter-interfaced generation units being integrated into distribution networks [1]. However, this evolution introduces new challenges for grid monitoring, control, and protection [2]. Grid-following inverters (GFLs) are frequently implemented in inverter-based resources to manage current injection while aligning with the phase angle and frequency of the grid voltage. Nonetheless, a significant presence of GFL affects system stability, especially under weak grid conditions associated with high grid impedances [3]–[5].

Moreover, a high penetration of Distributed Power Generation Systems (DPGS) impacts the line impedance within the distribution network. The performance of grid-connected converters is also known to be dependent on the characteristics of a grid impedance [6]. Grid impedance serves as a key parameter influencing the interaction among distributed energy sources and loads [7]–[9], as well as expressing the stability boundary for inverter controller parameters [10]–[12]. Multiple impedance-based stability assessment techniques for grid-connected inverters have been presented, including the Generalized Nyquist Criterion (GNC) [13], Singular-Value Criterion (SVC) [14], and d-Channel Criterion (DCC) [15], among others. These approaches incorporate a negative incremental resistance term within the d-q impedance framework to identify system stability boundaries. Moreover, the grid impedance is also an important factor in stability controller of grid connected inverter.

A research presents a modified virtual impedance model-based Phase Lock Loop (developed by same author with this paper), derived from [16] and referred to as MVIPLL, which incorporates line drop compensation using grid impedance data into the phase-locked loop (PLL) framework to counteract destabilising effects caused by the self-synchronisation loop. This model enables the voltage source converter to virtually synchronise with a point that demonstrates greater grid robustness. Additionally, the Advanced Angle Estimation based Kalman Filter with LQR current control (AAEKF-LQR) is described in [17] & [18], which integrates grid impedance parameters into the Kalman Filter approach for real-time instantaneous phase angle estimation. Both approaches utilise line drop compensation strategies informed by grid impedance characteristics to enhance inverter stability across varying grid conditions. Consequently, accurate grid impedance estimation is essential for the effective implementation of these research.

Grid impedance estimation in grid-connected inverters presents several technical challenges. One primary issue arises from harmonic distortion or disturbances in the measurements at the point of common coupling (PCC), which can significantly reduce the accuracy of the grid impedance estimation. Additionally, grid impedance may vary over time during system operation, necessitating methods that can provide fast and accurate estimation. In practice, impedance information is critical, as it influences the interaction between power converters and the grid, potentially leading to resonance or system instability [11], [19], [20]. Another important consideration involves integrating the grid impedance estimation method into inverter control strategies to maintain system stability. As a result, real-time or online estimation of grid impedance is essential for reliable inverter operation.

Multiple approaches have been developed for estimating grid impedance, which are generally categorised into active and passive techniques. Active methods are considered as

Phuoc Sang Nguyen, Ghavameddin Nourbakhsh, and Gerard Ledwich are with the School of Electrical Engineering and Robotics, Queensland University of Technology, Brisbane, QLD 4000, Australia

'invasive', whereas passive techniques are regarded as 'non-invasive'. The active approach injects one or more disturbance signals, either low-frequency [21] & [22] or high-frequency [23] & [24] into the grid. Grid impedance is then estimated using the voltage and current measurements at two steady-state operating points, recorded before and after the disturbance. Moreover, the active methods also use signal processing to derive the necessary information for estimating the equivalent grid impedance [6], [21], [22], [25]–[27]. However, the introduction of such disturbances can degrade power quality. and affect to stability performance. Additionally, in medium- or high-voltage networks, the equipment required to inject sufficient disturbances must be capable of delivering substantial power, which explains the approach impractical from a cost perspective [28].

On the other hand, the passive impedance estimation methods rely on observing existing non characteristic voltage and current harmonics within the grid, as detailed in [29] & [30]. These techniques derive the line impedance using means of the information during normal converter operation, without the need for external signal injection. As a result, these approaches avoid decreasing of power quality in the network. Several real-time grid impedance estimation techniques have been introduced, including extended Kalman filters [31], LCL filter excitation methods [32], and recursive least squares algorithms [33], discrete Fourier transform (DFT) [2], etc. In addition, the Discrete Fourier Transform (DFT) has been widely applied for impedance estimation because of its effective signal analysis capabilities, straightforward implementation, and low computational effort [34] & [35]. However, these passive methods have not been extensively examined in GFL operating under weak grid conditions or during variations in grid impedance. In grid-following (GFL) models, grid synchronisation is achieved through a Phase-Locked Loop (PLL) controller. However, studies have shown that under conditions of high grid impedance, PLL control can introduce low-frequency instability [36]–[38]. This instability is attributed to the appearance of a negative incremental resistance in the d–q impedance framework, as identified using the generalised Nyquist criterion [39]. This challenge necessitates methods capable of rapid and accurate grid impedance estimation, along with compatibility for integration with an advanced synchronisation controllers of grid-connected inverters to maintain stability performance.

This study presents a real-time grid impedance estimation method based on the Discrete Fourier Transform (GIE-DFT). The proposed approach is integrated with the Advanced Angle Estimation Kalman Filter combined with an LQR current controller (AAEKF-LQR), enabling the use of grid impedance information for instantaneous phase angle estimation. Numerical simulations are performed to evaluate the combined GIE-DFT and AAEKF-LQR method under high grid impedance scenarios and varying grid impedance during operation, focusing on the stability and dynamic behavior of a dual-source system. Discrete-domain simulations in the Matlab/Simulink environment are used to assess system stability. In addition, the effectiveness of the proposed method in mitigating external oscillation disturbances caused by a synchronous machine connected at the point of common coupling (PCC) is demonstrated.

The objectives of this work are to:

1) A grid impedance estimation technique based DFT is presented.
2) The proposed grid impedance estimation approach enables integration with AAEKF-LQR for precise instantaneous phase angle estimation
3) The combined use of the proposed estimation method and AAEKF-LQR addresses challenges associated with high grid impedance and ensures system synchronisation.

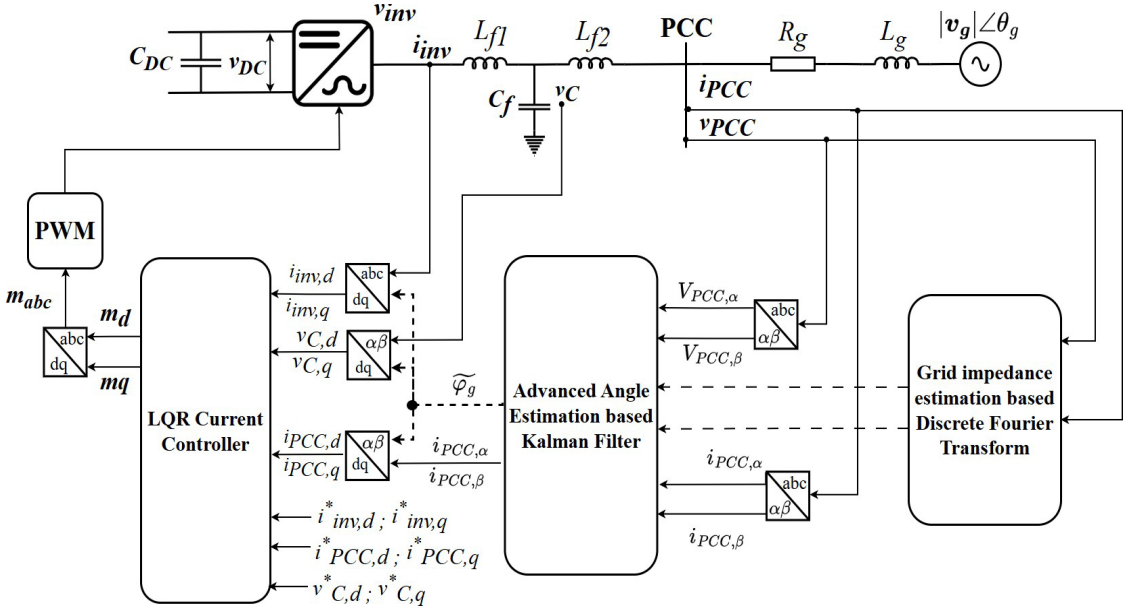

Fig. 1. Grid-following inverter model with AAEKF-LQR approach.

II. System Description and Control Schemes.

Fig. 1 shows a diagram of the GFL inverter model, which is integrated AAEKF-LQR controller and grid impedance estimation based DFT method into the system. The general system consists of an inverter terminal connected to a high-impedance grid through a LCL filter. This model contains five significant components: AC side inverter structure, AAEKF, LQR current controller, grid impedance estimation based DFT block and PWM generator block. The AAKF method is used to estimate the instantaneous grid phase angle φ_g. This instantaneous grid phase angle φ_g will be sent to the LQR current controller as a reference to inject current into the grid. Moreover, this current controller also regulates three states including inverter current, PCC current and capacitor voltage based on reference values to generate the output reference voltage to PWM block. The electrical system on the AC-side of GFL inverter model will be presented in a Synchronous Reference Frame (SRF), which is converted from abc-frame to Direct-quadrature-zero transformation dq-frame. The SRF equations of electrical system are presented dq-frame shown below.

$$\boldsymbol{x} = x_d + jx_q \tag{1}$$

III. Grid-following inverter model with AAEKF method Description

The AAEKF approach is employed to estimate the instantaneous grid phase angle φ_g, as detailed in [18]. The Kalman Filter acts as a state-optimal estimator and necessitates a state-space model for its operation. The corresponding state-space equations are presented as in (2). Furthermore, y_{KF} (t) is the PCC voltage in α-β frame.

$$\begin{cases} \dot{x_{KF}}(t) = \begin{bmatrix} 0 & -\omega \\ \omega & 0 \end{bmatrix} x_{KF}(t) \\ y_{KF}(t) = \begin{bmatrix} 1 & 0 \\ 0 & 1 \end{bmatrix} x_{KF}(t) + \begin{bmatrix} R_g & -\omega_g L_g \\ \omega_g L_g & R_g \end{bmatrix} u_{KF}(t) \end{cases} \tag{2}$$

The grid voltage in the alpha and beta frames are selected as the system state vector, defined as x_{KF} (t) = $[V_{g,\alpha}(t),\ V_{g,\beta}(t)]^T$. The components of grid voltage are represented as $V_{g,\alpha}(t) = |V_g| \cos[\varphi_g(t)]$, $V_{g,\beta}(t) = |V_g| \sin[\varphi_g(t)]$, $\varphi_g(t) = \omega_g t + \theta_g$, θ_g. The system input is given by u_{KF} (t) = $[i_{P\ CC,\alpha}(t),\ i_{P\ CC,\beta}(t)]^T$. Here, $\omega_g = 2\pi f_g$ denotes the grid angular frequency. Considering discrete-time implementation, $t = k_{KF}\ T_s$, with $T_s = 10^{-4}$ seconds as the sampling period and k_{KF} is the sampling instant. The estimated grid impedance is expressed as $\widehat{Z_g} = \widehat{R_g} + j\widehat{X_g} = \widehat{R_g} + j\omega\widehat{L_g}$.

To enable digital implementation of the Kalman Filter, the continuous-time state equations are converted into their discrete-time form. The resulting discrete state-space equations are presented as in (3).

$$\begin{cases} x_{KF}(\mathrm{k_{KF}} + 1) = \mathrm{A_d} x_{KF}(k_{KF}) + \mathrm{v}(k_{KF}) \\ y_{KF}(\mathrm{k_{KF}}) = \mathrm{C_d} x_{KF}(k_{KF}) + \mathrm{D_d u}(k_{KF}) + \mathrm{w}(k_{KF}) \end{cases} \tag{3}$$

Here, $\mathrm{v}(k_{KF})$ and $\mathrm{w}(k_{KF})$ denote the process and measurement noise, respectively. These variables are utilised in the definition of the process covariance matrix Q_{KF} and the measurement covariance matrix R_{KF} in (4).

$$Q_{KF} = E\left[\mathrm{v}(k_{KF})\ \mathrm{v}^T(k_{KF})\right] = q_{kf} I_2;\ R_{KF} = E\left[\mathrm{w}(k_{KF})\ \mathrm{w}^T(k_{KF})\right] \tag{4}$$

where I_2 denotes the 2×2 Identity matrix and q_{kf} represents a scalar value. The discrete system matrices and input matrices A_d, C_d and D_d are derived as described in [40], while the Kalman Filter algorithm implementation is based on [41]. In the proposed approach, the Kalman Filter estimator incorporates line drop compensation, and the estimated states x_{KF} (k) are calculated as follows.

$$\widehat{x_{KF}}(k) = \mathrm{A_d}\widehat{x_{KF}}(k-1) + K_{KF}(k)\ [y_{KF}(k) - \widehat{y_{KF}}(k)] \tag{5}$$

$$\widehat{y_{KF}}(k) = \mathrm{C_d}\widehat{x_{KF}}(k \mid k-1) + \mathrm{D_d} u_{KF}(k-1) \tag{6}$$

where K_{KF} (k) denotes the Kalman gain. Implementing the above Kalman Filter procedure provides estimates of the grid voltage in the α-β frame, from which the phase angle is derived as in (7).

$$\widehat{\varphi_g}(k) = \tan^{-1}\left[\frac{\widehat{V_{g,\beta}}(k)}{\widehat{V_{g,\alpha}}(k)}\right] \tag{7}$$

where $\bar{V}^{\alpha}$ $(k) = |\bar{V}| \cos[\bar{\varphi}\ (k)]$, $\bar{V}^{\beta}$ $(k) = |\bar{V}| \sin[\bar{\varphi}\ (k)]$ and $\hat{\varphi}(k) = \omega_g k T_s + \theta_g$ is the estimated instantaneous grid phase angle.

In addition, an LQR controller is designed to regulate the PCC current, inverter current, and capacitor voltage. The implementation follows the methodology outlined in [18].

IV. Grid impedance estimation method based

such as AAEKF-LQR and MVI-PLL models rely on grid impedance information for effective operation. To provide this information, the grid impedance estimation approach based on the Discrete Fourier Transform (DFT) utilises sequence data to determine accurate impedance values. The implementation procedure for this method is outlined as follows.

In the system, the measured PCC voltage and current in the three-phase abc frame are obtained. The objective is to extract the PCC voltage and current components corresponding to the fundamental frequency of $f = 50Hz$. Since the system operates in a digital environment with a sampling period of $T_s = 10^{-4}$ seconds, discretisation of the control process is necessary. A discrete-time signal $x_{P\ CC,m}[n]$, consisting of N equally spaced samples, can be represented as a sum of complex frequency components, as described in (8). Consequently, the Discrete Fourier Transform is applied to isolate the 50 Hz component of the PCC voltage and current in each phase a, b, and c, effectively filtering out contributions from other frequency components.

$$\widehat{x_{PCC,m}}[n] = \frac{2}{N}\sum_{k=0}^{N-1} X_{PCC,m} k_{DFT} e^{j2\pi kn/N} \tag{8}$$

Here, m represents each phase a, b, and c, while $k_{DF\ T}$ denotes the frequency index associated with the discrete frequency components. The discrete Fourier transform coefficients are derived using the following expression:

$$X_{PCC,m}[k_{DFT}] = \sum_{n=0}^{N-1} x_{PCC,m}[n] e^{-i2\pi k_{DFT} n/N} \quad (9)$$

Since only the values at the fundamental frequency of 50 Hz are required, the 50 Hz DFT window is selected, and the corresponding frequency index is set as $k_{DF\ T} = 1$. Accordingly, the discrete Fourier transform coefficient $X_{P\ CC,m}[1]$ is calculated. Therefore, the PCC voltage and current at 50 Hz for each phase a, b, and c are determined. The PCC voltage and current are decomposed into positive, negative, and zero sequence components using the equation derived from symmetrical component theory [42].

$$\begin{bmatrix} \widetilde{x_{PCC,a,0}} \\ \widetilde{x_{PCC,a,1}} \\ \widetilde{x_{PCC,a,2}} \end{bmatrix} = \frac{1}{3} \begin{bmatrix} 1 & 1 & 1 \\ 1 & \alpha & \alpha^2 \\ 1 & \alpha^2 & \alpha \end{bmatrix} \begin{bmatrix} \widetilde{x_{PCC,a}} \\ \widetilde{x_{PCC,b}} \\ \widetilde{x_{PCC,c}} \end{bmatrix} \quad (10)$$

Here the subscripts 0, 1, and 2 represent zero-, positive-, and negative-sequence components, respectively, and $a = e^{j2\pi/3}$ known as the $2\pi/3$ phase shift operator. Moreover, $x_{P\ CC,m}$ refers to the phasor form of $x_{PCC,m}$.

In this study, the three-phase abc components of PCC voltage and current are transformed into their positive-sequence, under the assumption that the negative and zero-sequence components are minimal and can be negligible. As a result, the phasor representations of PCC voltage and current in positive sequence are expressed as follows in (11) & (12), respectively.

$$\widetilde{V_{PCC,a,1}} = |\widetilde{V_{PCC,a,1}}|\angle\theta_{PCC,a,1} = \tfrac{1}{3} \times (\widetilde{V_{PCC,a}} + \alpha\widetilde{V_{PCC,b}} + \alpha^2\widetilde{V_{PCC,c}}) \quad (11)$$

$$\widetilde{I_{PCC,a,1}} = |\widetilde{I_{PCC,a,1}}|\angle\varphi_{PCC,a,1} = \tfrac{1}{3} \times (\widetilde{V_{PCC,a}} + \alpha\widetilde{V_{PCC,b}} + \alpha^2\widetilde{V_{PCC,c}}) \quad (12)$$

Subsequently, as illustrated in Fig. 1, the estimated grid impedance, observed from the PCC toward the grid side, is determined by applying Kirchhoff's Voltage Law.

$$\widehat{Z_g} = \widehat{R_g} + j\widehat{X_g} = \frac{\widetilde{V_{PCC,a,1}} - |V_{g,a,1}|\angle\theta_{g,a,1}}{\widetilde{I_{PCC,a,1}}} \quad (13)$$

the positive-sequence component of phase-a grid voltage. The estimated grid impedance is subsequently provided as an input to the AAEKF-LQR block for instantaneous grid angle estimation.

V. System Simulation and Analysis

A. Case study

This section evaluates the AAEKF-LQR model, and the grid impedance estimation method based on Discrete Fourier Transform (DFT) in terms of estimation accuracy, convergence time, and dynamic performance within a dual-source system framework. The model setup, including the electrical system and control strategy parameters, is outlined in Table I as referenced in [18]. According to [18], in order to achieve the achieve similar performance, the process covariance matrix is defined as $Q_{KF} = q_{kf}\ I_2$, q_{kf} is selected as 10^{-4}. While the measurement covariance matrix is defined as $R_{KF} = I_2$. Additionally, the weighting matrices for the LQR controller are set as $Q_{LQR} = diag([10^3, 10^3, 10^3, 10^3, 10, 10]^T)$ and $R_{LQR} = 10^{-2} I_2$. All parameters are expressed in per-unit to maintain consistency.

TABLE I
Parameters of control and electrical systems [10].

Parameter	Value	Parameter	Value
Rated power	110 KVA	Filter capacitance C_f	100 μF
Rated voltage	415 V	Filter inductance $L_{f1} = L_{f2}$	500 μH
Grid voltage v_g	1 pu	Reference inverter current i^*_{inv}	$1\angle 30^\circ$ pu
Grid frequency ω_g	$2\pi \times 50$ rad/s	DC source voltage v_{DC}	2.5 pu

The study also investigates transient behavior in the initial PCC voltage response under high grid impedance conditions. Two mitigation strategies are introduced to address transient effects: reducing the Kalman Filter gain and implementing a ramped current profile. Furthermore, the proposed grid impedance estimation method is assessed for accuracy and computational performance relative to the original system model. In addition, the AAEKF-LQR integrating with GIE-DFT methods are examined under conditions where grid impedance varies during operation, with emphasis on estimation accuracy and recovery capability. All simulations are performed using the MATLAB/Simulink platform with a sampling interval of 10^{-4} seconds.

This work assumes a constant DC link voltage. Two primary methods exist for mitigating harmonics in the DC link output voltage. The first involves employing a relatively large capacitor to suppress voltage ripples; however, this approach reduces the dynamic response of the PWM, slows the outer control loop, and results in delayed reference tracking [43] & [44]. The second method utilises a nonlinear control strategy to minimise small disturbances, enabling the use of a smaller DC link capacitor [45]–[47].

B. Validate the transient at the beginning

During the simulation of the original setup of AAEKF-LQR and GIE-DFT methods, transients are observed at the initial stage of the PCC voltage under high grid impedance conditions, particularly specifically when the grid impedance is set at $2\angle 60^\circ$ p.u [18]. This transient arises due to an inconsistency between the initial assumed grid impedance and its actual value, leading to a mismatch at the beginning of the estimation process. These transients may introduce issues in the system, such as affecting the reference tracking. In this scenario and system design, two approaches are identified as appropriate. The first involves reducing the Kalman Filter gain in the AAEKF block by adjusting the process noise covariance from $q_{kf} = 10^{-4}$ to 10^{-6} while maintaining the same measurement noise covariance R_{KF} . A reduction in the Kalman filter gain results in slower and smoother updates

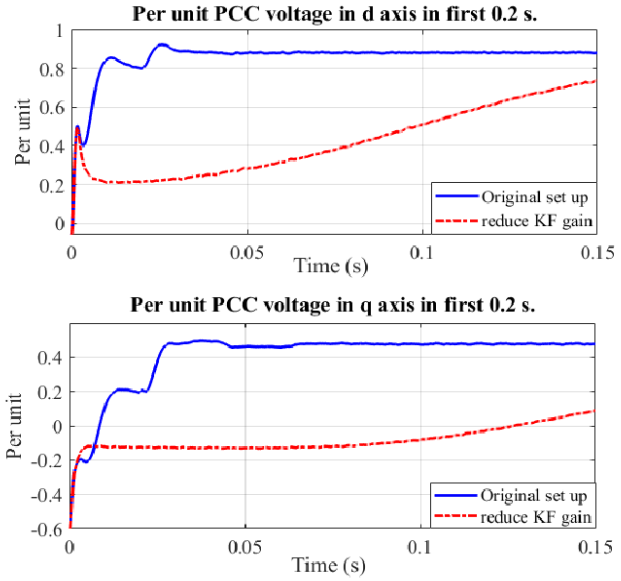

Fig. 2. Per unit PCC voltage in d-q axis in first 0.15 s Original vs reduce KF gain.

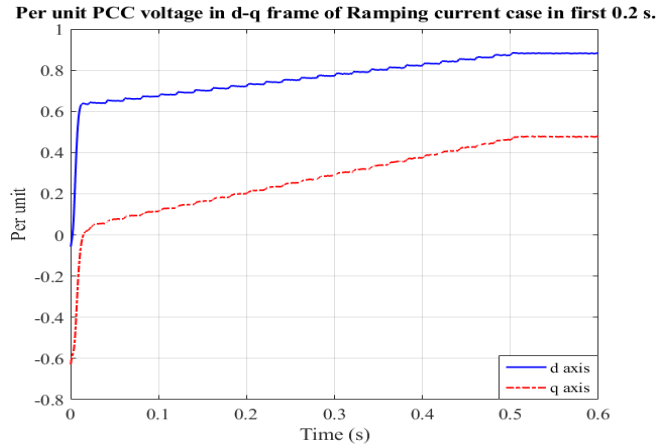

Fig. 3. Per unit PCC voltage in d-q frame of Ramping current case in first 0.6 s.

by relying more on the system model than on potentially noisy measurements. This dampens the Kalman Filter's reactivity, mitigates transient oscillations, contributing to enhanced system stability with a less aggressive response to sudden changes. The second approach involves applying a ramped reference PCC current in the current controller, gradually increasing the reference current from 0.1 p.u to 1 p.u in 0.02-second intervals over the first 0.5 seconds of operation. These simulation settings allow the grid impedance estimation based on DFT to initiate and operate from the start of the simulation. Gradual current ramping enables smoother system response by mitigating sharp transients and limiting inrush current, providing sufficient time for electrical components to react and preventing current spikes and potential instability. Additionally, this technique minimises overshoot and oscillations by reducing the likelihood of significant control errors from the Kalman Filter and LQR controller.

Fig. 2 & 3 illustrates the PCC voltage in both three-phase and dq frames, highlighting the initial transient responses

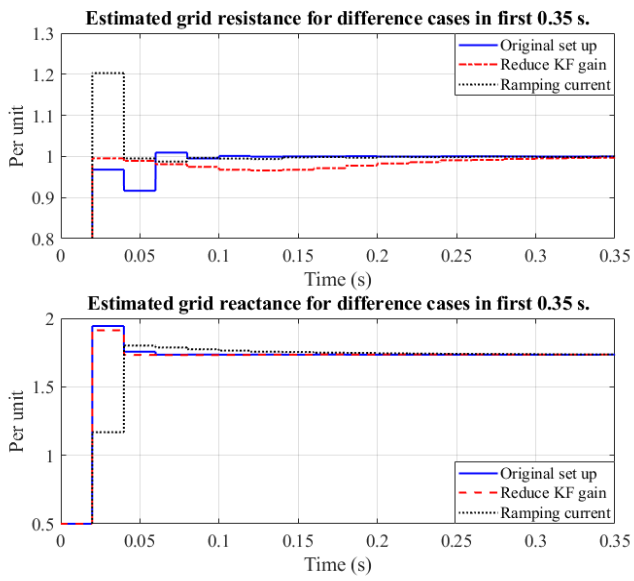

Fig. 4. Grid impedance estimation in first 0.35 s.

from three configurations: the original setup, a reduced KF gain scenario, and the ramping current technique. Under the original setup configuration, the PCC voltage in the dq frame exhibits oscillations that subside within 0.03 seconds. In contrast, the reduced KF gain configuration introduces a transient oscillation around 333 Hz, which dissipates after approximately 0.03 seconds. However, lowering the KF gain reduces the impact of new measurements on the state estimate, thereby slowing convergence and extending the time required to reach the desired steady-state values to approximately 0.4 seconds. In the case of the ramping current technique, the initial transient is effectively eliminated. Nonetheless, the system requires 0.5 seconds to reach the desired steady-state values.

C. Validate the grid impedance estimation by consider several testing cases

In these three testing methods, grid impedance estimation was also performed. Fig. 4 displays the estimated resistance ($\vec{R}_g$) and reactance ($\vec{X}_g$) of the grid impedance for each of the three approaches. In the original setup, the estimated grid impedance reaches the desired value in approximately 0.15 seconds. When the KF gain is reduced, the estimated grid impedance takes slightly longer, around 0.3 seconds, due to the increased error in the estimation of the instantaneous phase angle. As a result, it requires more time to converge, leading to higher grid impedance estimation errors and a more time-consuming estimation process. For the ramping current technique, the grid impedance estimation reaches the desired value in around 0.2 seconds. While the original setup provides the quickest grid impedance estimation. Because a higher KF gain places more weight on measured data rather than predicted values, enabling quicker adaptation to variations in observed data. This results in faster convergence and enhances the accuracy of PCC voltage and current inputs used in the grid impedance estimation method, thereby improving the overall

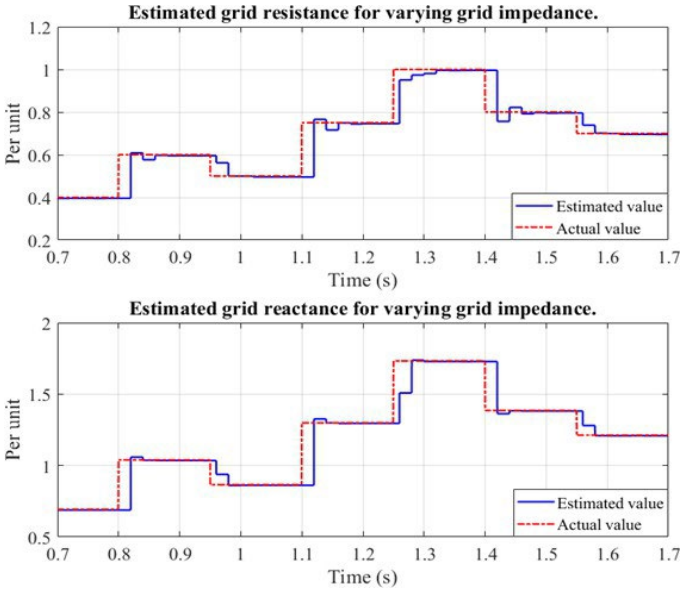

Fig. 5. Grid impedance estimation under varying levels of high grid impedance magnitude.

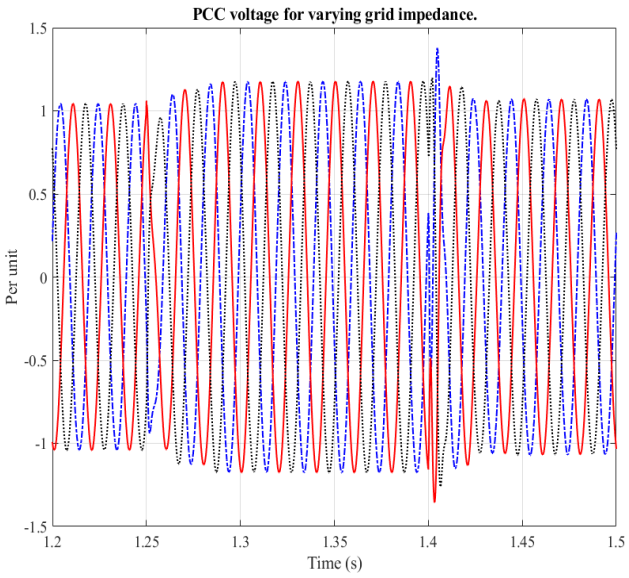

Fig. 6. Three phase PCC voltage under varying levels of high grid impedance magnitude from 1.2 s to 1.5 s.

precision of the estimated grid impedance. However, a high KF gain increases sensitivity to measurement noise, causing such disturbances to be more highly reflected in the updated state estimates. Consequently, in the original setup simulation, transients are observed at the initial stage of the PCC voltage in the dq frame, leading to a longer settling time compared to the other approaches.

For future analysis and simulation, the ramping current technique is selected due to its ability to eliminate initial transients, thereby reducing the risk of system disturbances. Additionally, this approach enables accurate estimation of grid impedance and contributes to overall system stability.

D. Analysis of Proposed grid impedance estimation based DFT Method + AAEKF-LQR under Sudden Grid Impedance Increases During the Simulation Process

This section employs discrete-domain simulation of the AAEKF-LQR and GIE-DFT methods to assess their effectiveness in terms of dynamic performance, stability, and estimation accuracy under varying levels of high grid impedance magnitude. The objective is to illustrate how different grid strengths influence system recovery, estimation precision, and convergence time, thereby providing critical insights into system behavior under diverse grid conditions. The ramping current technique is first executed to ensure system synchronisation is established prior to introducing a sudden variation in grid impedance for further analysis. Based on the findings from the previous section, the ramping current approach requires a minimum of 0.5 seconds to reach the reference PCC current. Therefore, the simulation is configured with a grid impedance of $0.8\angle 60^{\circ}$ pu maintained for 0.8 seconds to ensure proper system synchronisation. Following this, the grid impedance magnitude is changed every 0.14 seconds until the end of the simulation at 1.7 seconds. The sequence of impedance magnitudes applied is 1.2, 1.0, 1.5, 2.0, 1.6, and 1.4 per unit, respectively.

Fig. 5 illustrates the comparison between actual and estimated values of grid resistance and reactance. The results indicate that, following approximately four 50 Hz DFT windows (equivalent to 0.02 seconds), the grid impedance estimation method accurately determines the impedance values. Fig. 6 shows the PCC voltage waveform between 1.2 and 1.5 seconds. Transients occur during the switching of grid impedance magnitude from 1.5 to 2 per unit and subsequently from 2 to 1.6 per unit. Following each change, the PCC voltage stabilises and synchronises to the desired value within approximately 0.05 seconds. Consequently, the integration of the grid impedance estimation method based DFT with the AAEKF-LQR model during grid impedance variation effectively maintains control, contributing to system stability and synchronisation.

VI. Conclusion

This study presents a real-time grid impedance estimation approach based on the Discrete Fourier Transform, integrated with the Advanced Angle Estimation Kalman Filter and a Linear Quadratic Regulator (AAEKF-LQR) current controller, to enhance system stability under high grid impedance conditions. The estimation process achieves convergence to the desired impedance value in approximately 0.1 seconds. Furthermore, the proposed method demonstrates effective interaction with the AAEKF-LQR controller, enabling the system to recover and maintain stable performance under varying high grid impedance magnitudes.

References

[1] A. Monti, “Low inertia grids: Towards a power electronics-based power system,” in *2019 21st European Conference on Power Electronics and Applications (EPE’19 ECCE Europe)*, IEEE, pp. 1–1, ISBN: 907581531X.

[2] S. de Cavalcante Paiva, D. K. Alves, F. B. Costa, R. L. de Arau´jo Ribeiro, and T. O. A. Rocha, "Real-time impedance estimation in grid-connected photovoltaic system using the discrete fourier transform," in *2018 Workshop on Communication Networks and Power Systems (WCNPS)*, IEEE, pp. 1–5, ISBN: 1728106702.

[3] K. Givaki, D. Chen, and L. Xu, "Current error based compensations for vsc current control in weak grids for wind farm applications," *IEEE Transactions on Sustainable Energy*, vol. 10, no. 1, pp. 26–35, 2018, ISSN: 1949-3029.

[4] K. Givaki, D. Chen, L. Xu, and Y. Xu, "An alternative current-error based control for vsc integration to weak grid," in *2018 IEEE Power Energy Society General Meeting (PESGM)*, IEEE, pp. 1–5, ISBN: 1538677032.

[5] K. Givaki and L. Xu, "Stability analysis of large wind farms connected to weak ac networks incorporating pll dynamics," in *International Conference on Renewable Power Generation (RPG 2015)*, IET.

[6] M. Ciobotaru, R. Teodorescu, P. Rodriguez, A. Timbus, and F. Blaabjerg, "Online grid impedance estimation for single-phase grid-connected systems using pq variations," in *2007 IEEE Power Electronics Specialists Conference*, IEEE, pp. 2306–2312, ISBN: 1424406544.

[7] J. L. Agorreta, M. Borrega, J. Lo´pez, and L. Marroyo, "Modeling and control of *N* -paralleled grid-connected inverters with lcl filter coupled due to grid impedance in pv plants," *IEEE transactions on power electronics*, vol. 26, no. 3, pp. 770–785, 2010, ISSN: 0885-8993.

[8] J. H. Enslin and P. J. Heskes, "Harmonic interaction between a large number of distributed power inverters and the distribution network," *IEEE transactions on power electronics*, vol. 19, no. 6, pp. 1586–1593, 2004, ISSN: 0885-8993.

[9] Y. A.-R. I. Mohamed, "Mitigation of converter-grid resonance, grid-induced distortion, and parametric instabilities in converter-based distributed generation," *IEEE transactions on power electronics*, vol. 26, no. 3, pp. 983–996, 2010, ISSN: 0885-8993.

[10] J. Sun, "Small-signal methods for ac distributed power systems–a review," *IEEE Transactions on Power Electronics*, vol. 24, no. 11, pp. 2545–2554, 2009, ISSN: 0885-8993.

[11] J. Sun, "Impedance-based stability criterion for grid-connected inverters," *IEEE transactions on power electronics*, vol. 26, no. 11, pp. 3075–3078, 2011, ISSN: 0885-8993.

[12] H. Xu, J. Hu, and Y. He, "Operation of wind-turbine-driven dfig systems under distorted grid voltage conditions: Analysis and experimental validations," *IEEE Transactions on power electronics*, vol. 27, no. 5, pp. 2354–2366, 2011, ISSN: 0885-8993.

[13] A. G. MacFarlane and I. Postlethwaite, "The generalized nyquist stability criterion and multivariable root loci," *International Journal of Control*, vol. 25, no. 1, pp. 81–127, 1977, ISSN: 0020-7179.

[14] M. Belkhayat, *Stability criteria for AC power systems with regulated loads*. Purdue University, 1997, ISBN: 0591734397.

[15] R. Burgos, D. Boroyevich, F. Wang, K. Karimi, and G. Francis, "Ac stability of high power factor multi-pulse rectifiers," in *2011 IEEE Energy Conversion Congress and Exposition*, IEEE, pp. 3758–3765, ISBN: 1457705419.

[16] P. S. Nguyen, G. Nourbakhsh, and G. Ledwich, "A novel virtual impedance method for interfacing renewable to grid with high impedance," in *2023 IEEE PES Innovative Smart Grid Technologies-Asia (ISGT Asia)*, IEEE, pp. 1–5, ISBN: 9798350327748.

[17] P. S. Nguyen, G. Nourbakhsh, and G. Ledwich, "Advanced angle estimation using kalman filter for high impedance grid-following inverters stability," in *2024 IEEE PES Innovative Smart Grid Technologies Europe (ISGT EUROPE)*, IEEE, pp. 1–5, ISBN: 9798350390421.

[18] P. S. Nguyen, G. Nourbakhsh, and G. Ledwich, "Synchronising der inverters to weak grid using kalman filter and lqr current controller," *arXiv preprint arXiv:2507.01300*, 2025.

[19] X. Chen and J. Sun, "A study of renewable energy system harmonic resonance based on a dg test-bed," in *2011 Twenty-Sixth Annual IEEE Applied Power Electronics Conference and Exposition (APEC)*, IEEE, pp. 995–1002, ISBN: 142448085X.

[20] M. Liserre, R. Teodorescu, and F. Blaabjerg, "Stability of photovoltaic and wind turbine grid-connected inverters for a large set of grid impedance values," *IEEE transactions on power electronics*, vol. 21, no. 1, pp. 263–272, 2006, ISSN: 0885-8993.

[21] L. Asiminoaei, R. Teodorescu, F. Blaabjerg, and U. Borup, "Implementation and test of an online embedded grid impedance estimation technique for pv inverters," *IEEE Transactions on Industrial Electronics*, vol. 52, no. 4, pp. 1136–1144, 2005, ISSN: 0278-0046.

[22] A. V. Timbus, P. Rodriguez, R. Teodorescu, and M. Ciobotaru, "Line impedance estimation using active and reactive power variations," in *2007 IEEE Power Electronics Specialists Conference*, IEEE, pp. 1273–1279, ISBN: 1424406544.

[23] M. Sumner, B. Palethorpe, and D. W. Thomas, "Impedance measurement for improved power quality-part 1: The measurement technique," *IEEE Transactions on Power Delivery*, vol. 19, no. 3, pp. 1442–1448, 2004, ISSN: 0885-8977.

[24] Z. Staroszczyk, "A method for real-time, wide-band identification of the source impedance in power systems," *IEEE Transactions on Instrumentation and Measurement*, vol. 54, no. 1, pp. 377–385, 2005, ISSN: 0018-9456.

[25] A. Moallem, D. Yazdani, A. Bakhshai, and P. Jain, "Frequency domain identification of the utility grid parameters for distributed power generation systems," in *2011 Twenty-Sixth Annual IEEE Applied Power Electronics Conference and Exposition (APEC)*, IEEE, pp. 965–969, ISBN: 142448085X.

[26] A. V. Timbus, R. Teodorescu, and P. Rodriguez, "Grid impedance identification based on active power variations and grid voltage control," in *2007 IEEE Industry Applications Annual Meeting*, IEEE, pp. 949–954, ISBN: 1424412595.

[27] A. V. Timbus, R. Teodorescu, F. Blaabjerg, and U. Borup, "Online grid impedance measurement suitable for multiple pv inverters running in parallel," in *Twenty-First Annual IEEE Applied Power Electronics Conference and Exposition, 2006. APEC'06.*, IEEE, 5 pp. ISBN: 0780395476.

[28] H. Gu, X. Guo, D. Wang, and W. Wu, "Real-time grid impedance estimation technique for grid-connected power converters," in *2012 IEEE International Symposium on Industrial Electronics*, IEEE, pp. 1621–1626, ISBN: 1467301582.

[29] A. Bien, D. Borkowski, and A. Wetula, "Estimation of power system parameters based on load variance observations-laboratory studies," in *2007 9th International Conference on Electrical Power Quality and Utilisation*, IEEE, pp. 1–6, ISBN: 8469094416.

[30] K. O. H. Pedersen, A. H. Nielsen, and N. K. Poulsen, "Short-circuit impedance measurement," *IEE Proceedings-Generation, Transmission and Distribution*, vol. 150, no. 2, pp. 169–174, 2003, ISSN: 1350-2360.

[31] N. Hoffmann and F. W. Fuchs, "Minimal invasive equivalent grid impedance estimation in inductive–resistive power networks using extended kalman filter," *IEEE Transactions on Power Electronics*, vol. 29, no. 2, pp. 631–641, 2013, ISSN: 0885-8993.

[32] M. Liserre, F. Blaabjerg, and R. Teodorescu, "Grid impedance estimation via excitation of *LCL*-filter resonance," *IEEE Transactions on industry applications*, vol. 43, no. 5, pp. 1401–1407, 2007, ISSN: 0093-9994.

[33] S. Cobreces, E. J. Bueno, D. Pizarro, F. J. Rodriguez, and F. Huerta, "Grid impedance monitoring system for distributed power generation electronic interfaces," *IEEE Transactions on Instrumentation and Measurement*, vol. 58, no. 9, pp. 3112–3121, 2009, ISSN: 0018-9456.

[34] M. Bronzini, S. Bruno, M. De Benedictis, and M. La Scala, "Power system modal identification via wavelet analysis," in *2007 IEEE lausanne power tech*, IEEE, pp. 2041–2046, ISBN: 1424421896.

[35] S. Bruno, M. De Benedictis, and M. La Scala, "" taking the pulse" of power systems: Monitoring oscillations by wavelet analysis and wide area measurement system," in *2006 IEEE PES Power Systems Conference and Exposition*, IEEE, pp. 436–443, ISBN: 142440178X.

[36] X. Zhang, S. Fu, W. Chen, N. Zhao, G. Wang, and D. Xu, "A symmetrical control method for grid-connected converters to suppress the frequency coupling under weak grid conditions," *IEEE Transactions on Power Electronics*, vol. 35, no. 12, pp. 13 488–13 499, 2020, ISSN: 0885-8993.

[37] B. Wen, D. Dong, D. Boroyevich, R. Burgos, P. Mattavelli, and Z. Shen, "Impedance-based analysis of grid-synchronization stability for three-phase paralleled converters," *IEEE Transactions on Power Electronics*, vol. 31, no. 1, pp. 26–38, 2015, ISSN: 0885-8993.

[38] K. M. Alawasa, Y. A.-R. I. Mohamed, and W. Xu, "Active mitigation of subsynchronous interactions between pwm voltage-source converters and power networks," *IEEE Transactions on Power Electronics*, vol. 29, no. 1, pp. 121–134, 2013, ISSN: 0885-8993.

[39] B. Wen, D. Dong, D. Boroyevich, R. Burgos, P. Mattavelli, and Z. Shen, "Impedance-based analysis of grid-synchronization stability for three-phase paralleled converters," *IEEE Transactions on Power Electronics*, vol. 31, no. 1, pp. 26–38, 2015, ISSN: 0885-8993.

[40] L. Shieh, H. Wang, and R. Yates, "Discrete-continuous model conversion," *Applied Mathematical Modelling*, vol. 4, no. 6, pp. 449–455, 1980, ISSN: 0307-904X.

[41] B. D. Anderson and J. B. Moore, *Optimal filtering*. Courier Corporation, 2012, ISBN: 0486136892.

[42] J. D. Glover, M. S. Sarma, and T. J. Overbye, *Power system analysis and design*. Citeseer, 2011, ISBN: 1111425795.

[43] S. Gomez Jorge, J. A. Solsona, C. A. Busada, L. C. Aguirre-Larrayoz, M. Itsaso Mart´ınez, and G. Tapia-Otaegui, "Non-linear control of the power injected into a weak grid by a self-synchronized inverter," *arXiv e-prints*, arXiv: 2410.07102, 2024.

[44] X. Wu, S. K. Panda, and J. Xu, "Analysis and control of the output instantaneous power for three phase pwm boost rectifier under unbalanced supply voltage conditions," in *IECON 2006-32nd Annual Conference on IEEE Industrial Electronics*, IEEE, pp. 1–6, ISBN: 1509091556.

[45] G. Tapia-Otaegui, S. G. Jorge, J. A. Solsona, A. Susperregui, M. I. Mart´ınez, and C. A. Busada, "Complex-variable sliding-mode control of instantaneous complex energy and power for grid-tied inverter," *IFAC-PapersOnLine*, vol. 56, no. 2, pp. 451–457, 2023, ISSN: 2405-8963.

[46] J. A. Solsona, S. G. Jorge, and C. A. Busada, "A nonlinear control strategy for a grid-tie inverter that injects instantaneous complex power to the grid," in *2020 IEEE International Conference on Industrial Technology (ICIT)*, IEEE, pp. 895–900, ISBN: 1728157544.

[47] S. G. Jorge, J. A. Solsona, C. A. Busada, G. Tapia-Otaegui, A. S. Burguete, and M. I. M. Aguirre, "Nonlinear controller allowing the use of a small-size dc-link capacitor in grid-feeding converters," *IEEE Transactions on Industrial Electronics*, vol. 71, no. 3, pp. 2157–2166, 2023, ISSN: 0278-0046.